Mon. Not. R. Astron. Soc. **308**, 424–430 (1999)

Skew-symmetric solar p modes in low-ℓ BiSON* data

W. J. Chaplin,[1]† Y. Elsworth,[2] G. R. Isaak,[2] B. A. Miller[2] and R. New[3]
[1]*ESA Space Science Department, Solar System Division, ESTEC, 2200 AG Noordwijk, The Netherlands*
[2]*School of Physics and Astronomy, University of Birmingham, Edgbaston, Birmingham B15 2TT*
[3]*School of Science & Mathematics, Sheffield Hallam University, Sheffield S1 1WB*

Accepted 1999 April 7. Received 1999 April 7; in original form 1999 February 24

ABSTRACT

The p-mode oscillations of the Sun are manifestations of resonantly trapped acoustic waves propagating within its interior. The effective size of the resulting resonant cavity changes with the properties of the modes – the interaction of this phenomenon with a highly localized excitation source in the upper layers of the convection zone gives rise to skew-symmetric resonant profiles whose degree of asymmetry changes with frequency. Here, we have fitted low-angular-degree (low-ℓ) resonant p-mode peaks – in a power spectrum generated from 32 months of BiSON Doppler velocity observations of the visible solar disc – to a skew-symmetric formalism to account for this effect. We present the fitted frequencies, fine-structure spacings [$d_0(n)$ and $d_1(n)$] and mode-skewness estimates; and discuss the quantitative impact of fitting a skew, rather than symmetric, limit model. We also consider the reliability of the extracted parameters through the application of a useful statistical test, and extensive Monte Carlo fits to artificial data.

Key words: methods: data analysis – Sun: interior – Sun: oscillations.

1 INTRODUCTION

The resonant p-mode oscillations of the Sun constitute a well-established probe of the solar interior. By virtue of their differential penetration properties, the measurement of the frequencies of many thousands of modes allows one to constrain the hydrostatic and dynamic structure of much of the solar interior. The reliable estimation of these frequencies is clearly of the utmost importance – any systematic errors introduced in their determination may result in faulty inferences being drawn from analyses of such data.

The extraction of the frequencies usually proceeds by fitting the resonant peaks – in a Fourier transform of a coherent string of Doppler velocity or intensity observations of the solar disc – to a suitable model, usually a Lorentzian (e.g., see Woodard 1984). However, there is now clear observational evidence and a firm theoretical base which indicates that the peaks are skew symmetric (Gabriel 1992, 1995; Duvall et al. 1993; Roxburgh & Vorontsov 1995, 1997; Abrams & Kumar 1996; Rast & Bogdan 1997; Toutain et al. 1998; Rosenthal 1998; Korzennik 1998; Kumar & Basu 1999a,b).

Skew symmetry arises when a resonant system is excited by a well-localized source. For example, by seeking the resonant solutions of a simple square-well potential model – whose modes are excited by a delta-function source – one can readily produce varying degrees of asymmetry by altering the position of the source relative to the outer bound of the cavity and its nodes. In the solar case, p modes are excited in the outer layers of the convection zone. The upper bound of the acoustic cavity varies as a function of frequency (i.e., in response to the changing acoustic potential; see, for example, Unno et al. 1989); under the assumption that any variation in the depth of the excitation source as a function of mode frequency is small one might expect to see the extent of the asymmetry vary with frequency. This is indeed seen in power spectra of the solar acoustic resonances.

The interplay between the localized source and resonant cavity nevertheless fails to reproduce the reversal of asymmetry seen in Doppler velocity and intensity data. In order to achieve this, the modifying influence of a noise component that is distinct from – but nevertheless correlated with – the observed resonances appears to be required. Current proposals suggest the granular motion as the source, although specifics regarding which particular aspect of the motion is responsible do differ (Roxburgh & Vorontsov 1997; Nigam et al. 1998; Kumar & Basu 1999a,b).

Regardless of the details, the presence of skewness will give rise to systematic frequency errors if a symmetric model is assumed for the resonant limit spectrum. This effect is seen clearly by comparing frequencies extracted in this manner from intensity and velocity data (e.g., see Duvall et al. 1993; Toutain et al. 1997; Appourchaux et al. 1998a; Korzennik 1998). The skew symmetry is readily seen in the frequency domain at intermediate and high angular degrees – however, it is much less apparent at low ℓ, owing to the smaller number of available modes (each of which

* http://bison.ph.bham.ac.uk/
† E-mail: wjc@bison.ph.bham.ac.uk

has a 'ragged' appearance as a result of the stochastic nature of the excitation). Here, we demonstrate that a suitable analysis of BiSON data reveals significant skewness effects. We also consider the reliability of the fitted parameters, through both the application of suitable statistical tests, and extensive Monte Carlo simulations.

2 ANALYSIS

2.1 BiSON data

We have fitted the low-ℓ resonant peaks in a 32-month power spectrum, generated from velocity residuals collected between 1994 May 16 and 1997 January 10, i.e., at or near the solar activity cycle 22/23 minimum.

Adjacent $\ell = 2$ and 0, and $\ell = 3$ and 1 modes were fitted in pairs with maximum likelihood estimators (χ^2, two degrees-of-freedom statistics assumed) as rotationally split, skew-symmetric multiplets with an associated flat background offset. The first, temporal sidebands were also included in the model. The power, P, in each azimuthal mode component has been modelled according to (Nigam & Kosovichev 1998):

$$P(\xi) = \left(\frac{H}{1+\xi^2}\right)\cdot[(1+\alpha\xi)^2 + \alpha^2], \qquad (1)$$

where

$$\xi = 2(\nu - \nu_0)/\Delta\nu,$$

and ν_0 is the frequency of the Lorentzian component, $\Delta\nu$ its width, and H its height. The parameter α is essentially the 'fractional' asymmetry of the mode. This formalism reduces to a pure Lorentzian for $\alpha \rightarrow 0$. Note that it is an approximation to a function obtained by solving a suitable, bounded wave equation, and is valid only in the vicinity of the resonance.

We used a multidimensional direction-set minimization algorithm (Press et al. 1992) to perform the fitting, by maximizing an appropriate log-likelihood function. At frequencies up to $\sim 3500\,\mu$Hz, the following parameters were varied iteratively until they converged to their best-fitting values:

(i) A frequency for each mode.

(ii) A single skewness parameter (the m components of the modes in the pair are all assumed to have the same skewness).

(iii) A single parameter describing a symmetric rotational splitting pattern for each mode (not applicable at $\ell = 0$).

(iv) A single width for both modes (i.e., each m component was assumed to have the same width in both multiplets constituting the low-ℓ pair).

(v) A single height – that of the outer, sectoral m components – for each mode. The relative m-component height ratios were assumed to take fixed values (Christensen-Dalsgaard 1989).

(vi) A single relative sideband height for each mode. At low frequencies, the relative sideband heights were fixed according to the characteristics of the window function.

(vii) And a flat, background offset for the whole fit.

The natural logarithms of the height, width and background terms were varied – not the straightforward parameter values themselves – in order to give a quasi-normal fitting distribution. Estimates of the formal uncertainties in each parameter could then be determined from the inverse of the Hessian matrix describing the hypersurface of the fit.

At frequencies above $3500\,\mu$Hz: the fractional sideband heights were fixed, according to the characteristics of the window function; and the rotational splitting pattern was fixed for all modes, with a constant synodic spacing (appropriate to $\Delta|m| = 1$) of 400 nHz. (For a more in-depth discussion of the fitting low-ℓ data, see Toutain & Appourchaux 1994; Chaplin et al. 1998.)

2.2 Monte Carlo simulations

We have performed an extensive series of Monte Carlo simulations in order to test the validity of the mode-fitting procedures applied to the real velocity data. Many artificial mode pairs (i.e., $\ell = 2/0$ and 3/1) were generated and then fitted over a range of simulated n matching that fitted in the BiSON spectrum. At each n, the input characteristics to each mode pair (e.g., frequencies, splittings, widths, signal-to-noise ratio, etc.) were taken from a data base of BiSON values. For one subset of the simulations, the artificial modes were given skew symmetries, fixed according to a smooth function fitted through the estimates shown in Fig. 1 (see Section 3.1).

The generation of each pair realization proceeded as follows. Once the limit spectrum had been constructed, through the use of equation (1) in the frequency domain, the real and imaginary parts of the spectrum were generated by applying Gaussian noise to the limit values. The time series of this spectrum was then recovered by taking the inverse Fourier transform, and modulated by the 32-month BiSON window function. (For one subset, we did not apply the window function.) Additional normally distributed noise was also added in the time domain in order to give realistic signal-to-noise ratios at low frequencies. The power spectrum computed from the resulting time series was then fitted, as described in Section 2.1. Note that for some of the simulations, we fitted symmetric Lorentzians, rather than the skew-symmetric Nigam & Kosovichev formalism. For each simulated low-ℓ pair at a given n, this procedure was repeated some 250 times, giving 250 fits to independent realizations of the same mode-pair limit spectrum. From these, we determined a weighted mean of each fitted parameter, through the use of the formal uncertainties recovered by the fitting procedure as weights.

3 RESULTS

3.1 Fitted skewness in the BiSON spectrum

In Fig. 1 we show the skew-symmetry parameter estimates, α, extracted by fitting the 32-month spectrum. The size of – and observed trend in – the fitted skewness parameters is extremely similar to that found by Toutain et al. (1998) from the analysis of low-ℓ MDI velocity data.

3.1.1 Significance of the extracted skewness estimates

We have tested the significance of fitting a skew, rather than symmetric, function to these data by performing a log-likelihood difference test to each fit (Appourchaux et al. 1995). In addition to the skew-model fits, we also fitted symmetric Lorentzian profiles to the resonant peaks (i.e., by fixing $\alpha = 0$ in equation 1). With j parameters varied in each symmetric fit, and $j+1$ parameters varied for each skew fit – the extra parameter characterizing the skewness of the modes in the pair – each yielded at convergence a measure of the logarithm of the likelihood of the best-fitting model, $\mathscr{L}_j$ and $\mathscr{L}_{j+1}$ respectively. Since the difference $-2(\mathscr{L}_j - \mathscr{L}_{j+1})$ is

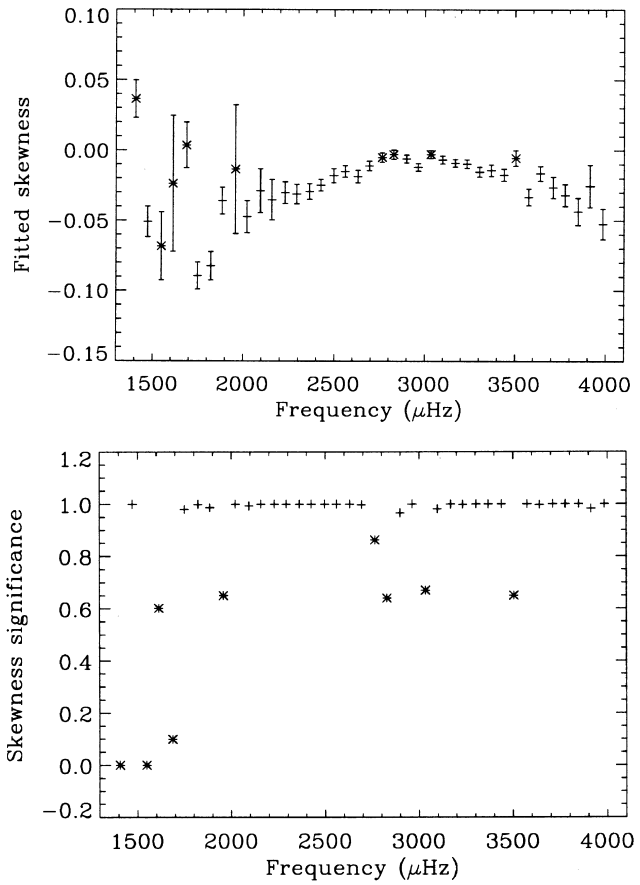

Figure 1. Upper panel – variation of the mode-skewness parameter α (see equation 1) extracted from fits to the 32-month BiSON spectrum. Each datum corresponds to the fitted skewness for alternating $\ell = 2/0$ and 3/1 low-ℓ pairs. Lower panel – significance of fitting the extra skewness parameter to each mode pair. Those fits for which the significance is noticeably below unity are marked by an asterisk in both panels.

distributed as χ^2 with one degree of freedom (corresponding to the extra fitted parameter; see Appourchaux et al. 1995 and references therein), the significance of introducing the extra parameter is readily determined. The lower panel in Fig. 1 shows the corresponding probabilities for fits to the BiSON spectrum. This plot provides firm evidence for there being significant skewness in the observed resonant profiles. Those fits for which the calculated probability is noticeably below unity have been marked by asterisks in both panels. One can see that by removing these data, much of the spurious scatter present at low frequencies disappears. (An additional high-frequency datum, clearly out-of-line with the other values in its vicinity, is also removed.) Given that the inferred skewness tends to very small values near the centre of the spectrum, it is not surprising that three of the fits fail the test in this region also.

3.1.2 Scatter and bias in the extracted skewness estimates

Returning to the points that remain at low frequencies in Fig. 1, these do nevertheless still suggest the presence of additional scatter, over and above that implied by the plotted formal error bars (each of which is derived from the Hessian of the corresponding fit). Intuitively this is not surprising given the small size and decreasing magnitude of the mode linewidths at low n, and the fixed resolution of the spectrum.

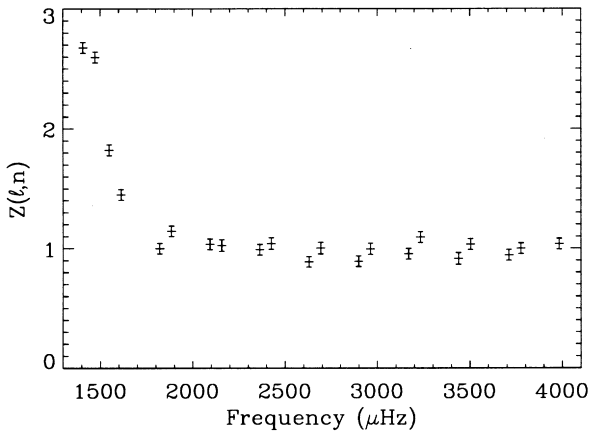

Figure 2. Ratio of the external to internal errors in the best-fitting skewness parameter, $\alpha(\ell, n)$, derived from Monte Carlo simulations of artificial data. Each plotted datum has been derived from fits to some 250 independent mode-pair realizations generated at each (ℓ, n).

To test this quantitatively, we performed a series of Monte Carlo simulations, as outlined in Section 2.2. Of relevance here, we analysed the results of fitting simulated skew-symmetric low-ℓ pairs – with the 32-month window function included – to a skew-symmetric model. We note once more that the input skewness values used to construct the artificial modes were chosen in order to mimic those in Fig. 1. For N simulations performed at each modelled (ℓ, n), we computed the quantity:

$$Z(\ell, n) = \sqrt{\frac{1}{(N-1)} \sum_{i=1}^{N} \frac{[\alpha_i(\ell, n) - \bar{\alpha}(\ell, n)]^2}{\delta\alpha_i(\ell, n)^2}},$$

and its associated uncertainty

$$\delta Z(\ell, n) = [2(N-1)]^{-1/2}.$$

In the above: $\alpha_i(\ell, n)$ are the best-fitting skewness values for the N independent, modelled data realizations; $\bar{\alpha}(\ell, n)$ their mean; and $\delta\alpha_i(\ell, n)$ the associated formal uncertainties, derived from the Hessian of each fit. $Z(\ell, n)$ is a measure of the ratio of the external and internal errors associated with each set of simulations – if the Hessian-derived error is a reliable estimate of the true uncertainty, then $Z(\ell, n)$ should lie close to unity. In Fig. 2 we plot $Z(\ell, n)$ determined from the $N = 250$ artificial mode-pair realizations fitted at each (ℓ, n). For much of the frequency range, $Z(\ell, n)$ is indeed near unity. However, at frequencies progressively below $\sim 2000\,\mu$Hz, the increasing size of $Z(\ell, n)$ indicates that the best-fitting skewness values are more scattered than implied by the Hessian-derived formal errors. This is consistent with the appearance of the low-frequency end of Fig. 1. Clearly, superior resolution is required at low n in order to infer reliably the form of the observed resonant profiles.

While the above bears upon the scatter we may expect in the fits at each (ℓ, n), it says nothing regarding any underlying bias that might be present in those estimates. To test this, we computed the weighted mean of the N best-fitting skewness values at each simulated (ℓ, n), and compared these with the input values used to construct the artificial modes. In addition, we also determined means for artificial time series constructed with a 100 per cent fill.

The artificial $\ell = 2/0$ fitted means match well with the true (input) skewness values, with an rms deviation over the entire spectrum of ~ 4 per cent. The $\ell = 3/1$ differences display similar

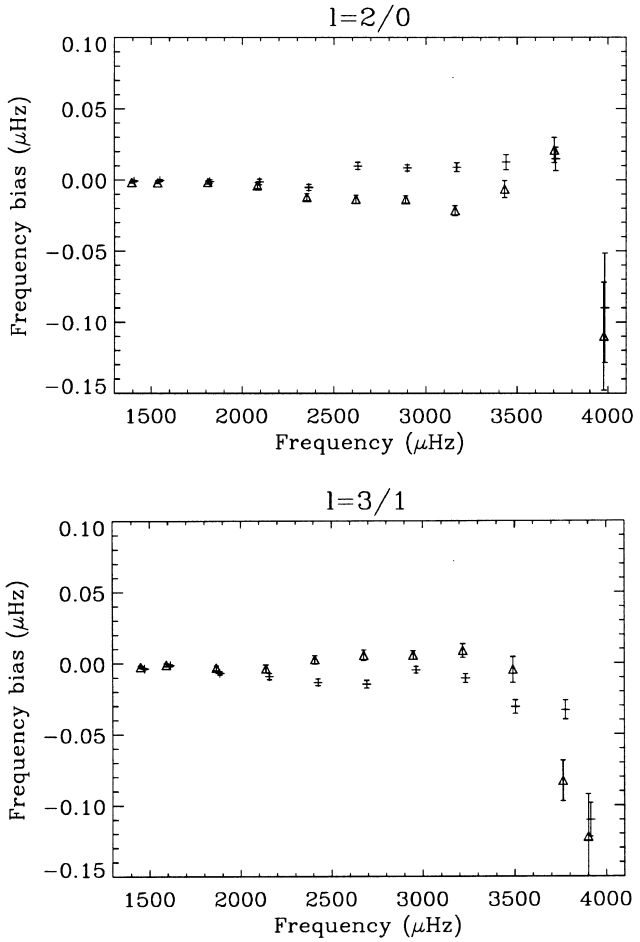

Figure 3. Differences between the mean, fitted frequencies from the 250 artificial mode simulations made at each (ℓ, n) and the actual input frequencies. Upper panel – differences for simulated $\ell = 2$ (triangles) and 0 (crosses) modes; lower panel – those for $\ell = 3$ (triangles) and 1 (crosses). The error bars are the uncertainties in the plotted weighted means, as determined from the 250 independent fits used to calculate each datum.

behaviour up to $\approx 3100\,\mu$Hz – at frequencies above this, there is a clear tendency for the fitted skewness to be more positive than the actual skewness by a fractional amount that rises to ~ 20 per cent at $\approx 3500\,\mu$Hz, before tailing off slightly at higher n. Interestingly, indications of this behaviour are present in the fitted BiSON values in Fig. 1. Here, the $\ell = 3/1$ values at high frequencies tend to be more positive than their nearest $\ell = 2/0$ counterparts. We note that the 100 per cent fill simulations do not show any indications of similar bias. This clearly emphasizes the need for data sets that are as well-filled as possible in order to enable one to study subtle aspects of the acoustic mode spectrum.

3.1.3 Effect upon fitted eigenfrequencies

Next, we investigated how systematic errors in the estimated skew symmetries mapped to errors in the determination of the associated eigenfrequencies, again through the use of artificial data. The differences between the mean, fitted frequencies from the 250 window-function-modulated simulations made at each (ℓ, n) and the actual input frequencies are plotted in Fig. 3. The upper panel displays the differences for simulated $\ell = 2$ (triangles) and 0 (crosses) modes; and the lower panel those for

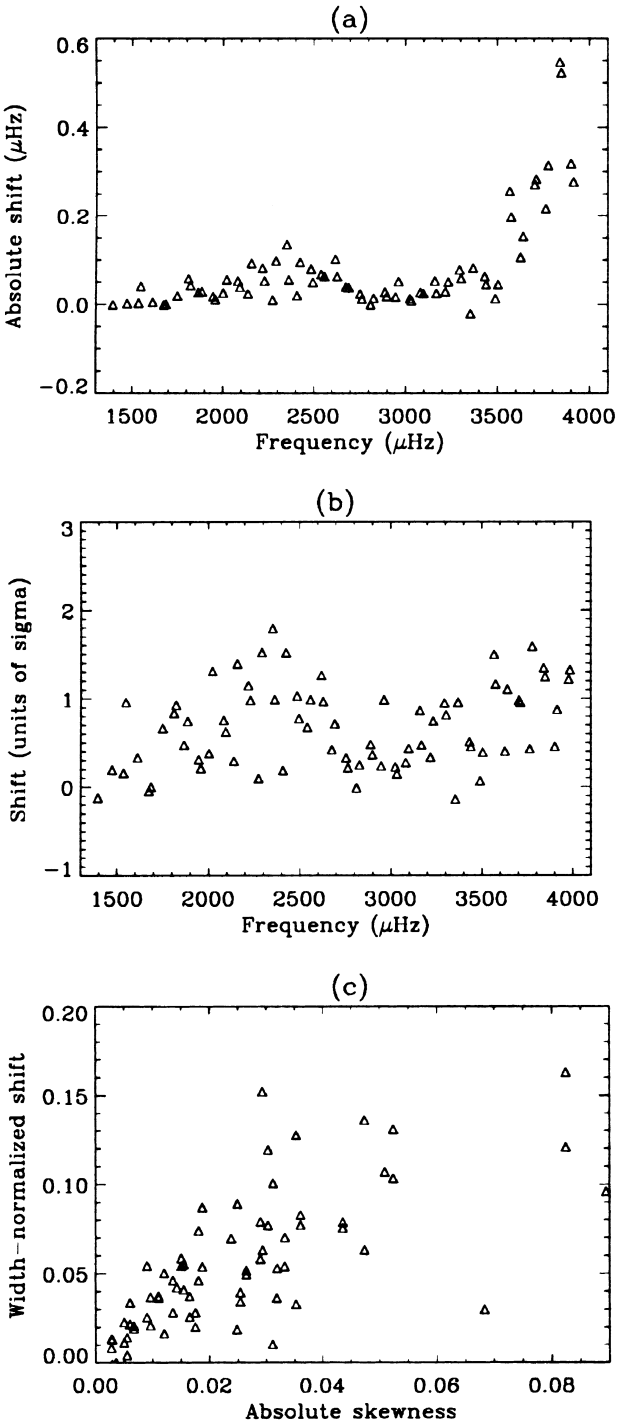

Figure 4. Frequency differences for $0 \leq \ell \leq 3$ found by fitting skew-symmetric (formalism of Nigam & Kosovichev 1998, defined in equation 1) and symmetric (Lorentzian) models to the same data set (plotted in the sense skew minus symmetric). In: (a) – the straight differences; in (b) – the differences normalized by the combined error at each (ℓ, n); and in (c) – the differences normalized by the skew-fit FWHM line width, $\Delta\nu(\ell, n)$, plotted as a function of the absolute skewness, $|\alpha(\ell, n)|$, returned from the skew fit.

$\ell = 3$ (triangles) and 1 (crosses). The error bars are the uncertainties in the plotted weighted means, as determined from the 250 independent fits used to calculate each datum.

Over most of the fitted range, the implied bias in the frequency

estimates is of the order of ~20 nHz or less. The bias in the $\ell = 3$ and 1 fits tends to more negative values at high n. This is consistent with the bias in the $\ell = 3/1$ skew-symmetry estimates, as discussed above in Section 3.1.2. Here, the frequencies are pulled by as much as $\sim -0.15\,\mu$Hz at ~4000 μHz, values which are still less than the line width at these frequencies. The lack of any severe bias in the $\ell = 2/0$ fits persists up to $\ell = 2$, $n = 27$ and $\ell = 0$, $n = 28$ – the mean fitted frequencies for the modes in this simulated pair are, however, clearly offset.

We also performed a similar subset of simulations and fits, but with no window function applied in the time domain. These results showed no inherent bias. The results in Fig. 3 do therefore suggest that fits to the real data may be slightly biased at high n. However, we note that the magnitude of the implied bias is at a level below the formal mode-frequency uncertainties fixed by the 32-month period of observation and the lifetimes of the modes themselves (see Section 3.2 and Table 1 below). Clearly, estimates from individual 32-month spectra will be distributed about the mean, bias values.

We conclude by noting that our experience with artificial data suggests strongly that any inherent bias introduced is quite subtle, and depends to some extent on the specific characteristics of the window function that is applied to the data set, and its complex interaction with the fitting model in the frequency domain.

3.2 Fitted BiSON eigenfrequencies

As indicated in Section 3.1, in addition to fitting the skew-symmetric profile, we also fitted the modes with symmetric Lorentzian profiles. Fig. 4(a) shows the difference in the fitted frequencies (in the sense skew minus symmetric). The distribution of points in (a) is similar to that observed by Rhodes et al. (1997), who performed a similar exercise with medium-ℓ MDI data. In Fig. 4(b), the differences have been normalized by the combined error bar – the bias, while clearly present, is comparable to the size of the uncertainties on the individual frequency determinations (which are appropriate to the 32-month integration period). The trend observed in (a) can be 'linearized' (e.g., Abrams & Kumar 1996) by normalizing the shift by the fitted full width at half-maximum (FWHM) line width, $\Delta\nu$, and plotting this as a function of the fitted skewness (or here in (c), the absolute skewness). If one fits a straight line to these data, the returned gradient is 1.41 ± 0.20. Note that a much less scattered linear trend is obtained from data with a 100 per cent duty cycle.

Table 1 lists the skew-model-fitted BiSON frequencies. Where fits at low frequencies failed the log-likelihood difference test (see Section 3.1), we have listed the symmetric-model-fitted frequencies in preference. Given the narrow width of these modes, the difference in the frequencies is small, e.g., see Figs 4 (a) and (b). We note that the listed frequencies have not been corrected for solar-cycle-induced shifts. However, we note that the period spanned by the observations covers that near the activity minimum at the cycle 22/23 boundary.

We have compared the frequencies in Table 1 with those given by Toutain et al. (1998), who fitted the Nigam & Kosovichev skew-symmetric formalism, at $0 \leq \ell \leq 2$, to a 679-day MDI spectrum. Any systematic shifts arising from the non-contemporaneous nature of the two data sets should be minimal. We have calculated the mean 10.7-cm radio flux over the period of both sets of observations, and find agreement to within three standard RF units. (The notional activity minimum is 65 RF units; a full discussion of the radio-flux activity dependence of the low-ℓ eigenfrequencies, and the issues associated with correcting p-mode frequencies for the solar cycle, can be found in Chaplin et al. 1998.)

The level of agreement between the listed eigenfrequencies is good at low and moderate n. Of the 45 differences at $n < 24$, six are significant at 2σ or more (differences normalized by the combined uncertainties). However, at higher n, there is clear

Table 1. Raw, low-degree solar p-mode eigenfrequency set, derived from fitting a skew-symmetric model to a single, 32-month BiSON frequency spectrum. This was generated from data collected at or near the solar activity minimum. Note that these entries have not been corrected for solar cycle effects. The listed uncertainties are the formal errors derived from the inverse of the Hessian matrix associated with each fit.

	Mode frequency (μHz)			
n	$\ell = 0$	$\ell = 1$	$\ell = 2$	$\ell = 3$
8	…	…	1394.659 ± 0.008	…
9	…	1472.828 ± 0.007	1535.857 ± 0.012	…
10	1548.328 ± 0.037	1612.715 ± 0.009	1674.543 ± 0.015	…
11	1686.570 ± 0.019	1749.303 ± 0.019	1810.350 ± 0.039	1865.289 ± 0.038
12	1822.227 ± 0.034	1885.112 ± 0.029	1945.740 ± 0.038	2001.200 ± 0.050
13	1957.407 ± 0.027	2020.794 ± 0.030	2082.052 ± 0.051	2137.804 ± 0.057
14	2093.494 ± 0.046	2156.760 ± 0.051	2217.743 ± 0.052	2273.471 ± 0.065
15	2228.696 ± 0.040	2291.954 ± 0.047	2352.162 ± 0.052	2407.722 ± 0.073
16	2362.824 ± 0.042	2425.617 ± 0.046	2485.874 ± 0.055	2541.657 ± 0.068
17	2496.172 ± 0.048	2559.139 ± 0.047	2619.724 ± 0.059	2676.242 ± 0.062
18	2629.680 ± 0.048	2693.310 ± 0.040	2754.374 ± 0.053	2811.426 ± 0.058
19	2764.088 ± 0.041	2828.058 ± 0.042	2889.556 ± 0.042	2946.981 ± 0.049
20	2898.953 ± 0.036	2963.393 ± 0.039	3024.662 ± 0.042	3082.252 ± 0.068
21	3033.749 ± 0.040	3098.111 ± 0.042	3159.918 ± 0.042	3217.814 ± 0.060
22	3168.527 ± 0.038	3233.222 ± 0.049	3295.088 ± 0.059	3353.381 ± 0.100
23	3303.480 ± 0.052	3368.586 ± 0.063	3430.979 ± 0.088	3489.528 ± 0.137
24	3438.973 ± 0.073	3504.038 ± 0.087	3567.071 ± 0.126	3626.061 ± 0.191
25	3574.987 ± 0.121	3640.307 ± 0.104	3703.208 ± 0.207	3762.638 ± 0.372
26	3710.664 ± 0.216	3776.859 ± 0.151	3840.098 ± 0.307	3900.509 ± 0.528
27	3847.579 ± 0.300	3913.392 ± 0.251	3977.242 ± 0.653	…
28	3984.403 ± 0.722	…	…	…

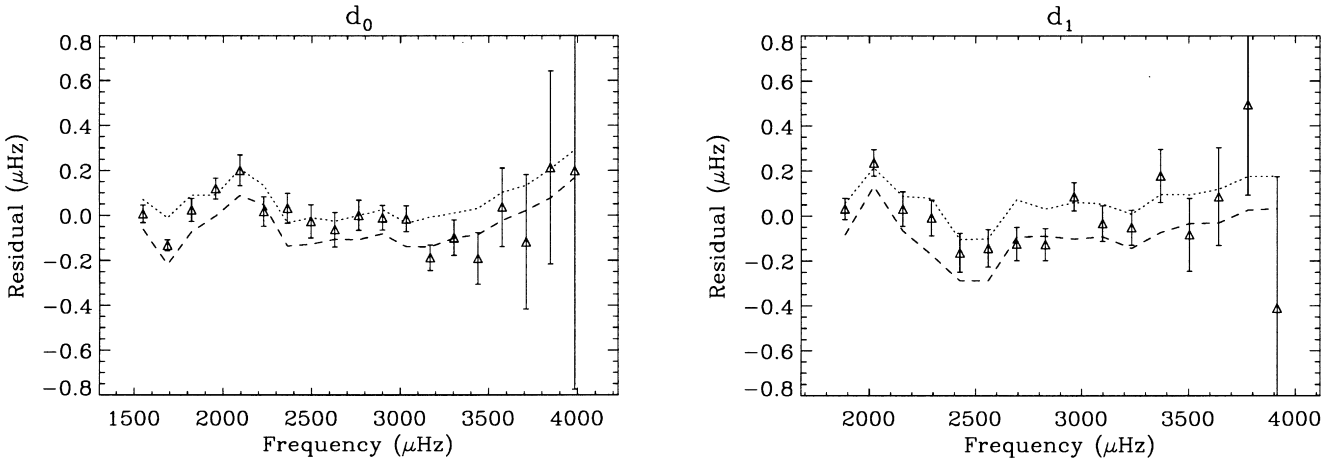

Figure 5. The left-hand [$d_0(n)$] and right-hand [$d_1(n)$] plots show the residuals generated by fitting a straight line, as a function of radial order n, to the BiSON spacings, and then subtracting this from the three data sets shown. The data with error bars were calculated from the BiSON frequencies in Table 1; the dotted line indicates values calculated from model 'S' (Christensen-Dalsgaard et al. 1996), which includes heavy-element settling but neglects the effects of turbulence; and the dashed line indicates predictions from model 4 of Christensen-Dalsgaard et al. (1993), which includes heavy-element settling with turbulent mixing.

evidence for the onset of a systematic trend, with the BiSON-minus-MDI differences becoming increasingly negative. This effect is most severe at $\ell = 1$, where the four highest n pairs all show marked offsets. The fact that we have uncovered similar behaviour in our simulations (see Fig. 3) argues in favour of much of this arising from the complex interaction of the BiSON window function with the BiSON fits. Again, we stress that our simulations failed to reproduce similar offsets in the absence of a window function. However, the magnitude of the differences shown at $\ell = 1$ – which reach $\approx -1.5\,\mu$Hz at $n = 27$ – is puzzling.

Our simulations appear to mark out such offsets as high$-\sigma$ outliers (see Section 3.1.3). For example, consider the values at $n = 27$: given the data in Fig. 3, a rare, 4σ deviation would be expected to have size $\approx -1.0\,\mu$Hz. Clearly, the simulations may not fully reflect the true nature of the bias present in fits to the real data. Nevertheless, if we compare our high-n, $\ell = 1$ frequencies with other recently published values from LOI and GONG data (Appourchaux et al. 1998b; Rabello-Soares & Appourchaux 1999) – having made suitable empirical corrections based upon our extensive simulations to allow for the fitting of Lorentzians and the type of observation, i.e., intensity or velocity – we find that the BiSON values are in better agreement with these than the Toutain et al. fits. So, while we accept that some of the bias will be the result of window function contamination of the BiSON frequency spectrum, we suggest that this does not wholly account for the spurious magnitude of the high-n differences.

3.3 BiSON fine-structure spacings

Here, we follow the convention of Chaplin et al. (1997) in comparing the fine-structure spacings, $d_0(n)$ and $d_1(n)$, determined from the frequencies in Table 1 with those calculated from models that include the effects of helium and heavy-element settling. We fitted a straight line to the BiSON spacings expressed as a function of the radial order n (Elsworth et al. 1990) and then subtracted the best-fitting line from both the data and the model values. This removes the marked slope in the spacings, and serves to provide a better visual comparison of the data. In Fig. 5 we plot the resulting residuals for the BiSON data and two solar models. The dotted line in each panel shows spacings determined from model 'S' of Christensen-Dalsgaard et al. (1996), which includes heavy-element settling but neglects the effects of turbulence; while the dashed line indicates predictions from model 4 of Christensen-Dalsgaard, Proffitt & Thompson (1993) which incorporates both heavy-element settling and some turbulent mixing. Both panels illustrate that a straight-line parametrization of the observed spacings is no longer adequate, given the precision in the frequencies that is achievable with current helioseismic data (see also Chaplin et al. 1997, and discussions therein). Of interest here, the observed spacings do broadly follow the trends present in the modelled data. However, it is rather difficult to choose a preferred model, given the magnitude of the errors on the BiSON spacings and the frequency offset between the modelled data, both of which are comparable in size.

In addition, we also tested whether the skew-symmetric BiSON spacings presented in Fig. 5 provide a better match to the models than those generated by fitting a symmetric (Lorentzian) model. As one might expect, while differences in the frequencies may be regarded as a first-order correction, those in the fine-structure spacings are of a higher order. As such, we expect, and indeed find, no clear difference in the mean difference residuals computed between the skew and symmetric fits and the models respectively over all available n. We also analysed the scatter in the BiSON-skew-minus-model and BiSON-symmetric-minus-model differences by computing the χ^2 statistic for a simple mean offset describing the two sets of residuals. There is a slight suggestion of a reduction in the scatter of the skew-fit differences for d_0; the symmetric and skew-fit differences at d_1 do, however, return similar test values.

The artificial simulations outlined in Section 2.2 do suggest a slight bias in the fine spacings calculated from the fitted frequencies when the real BiSON window function is applied. The mean $\ell = 2/0$ spacings overestimate, while the mean $\ell = 3/1$ spacings underestimate, the true (input) values in the simulations by an amount that rises to $\sim 0.02\,\mu$Hz at high frequencies. This is at a level below the formal errors shown in Fig. 5.

ACKNOWLEDGMENTS

We would like to thank all those who are – or have been –

associated with the BiSON global network. In particular: H. K. Williams, J. Litherland, A. Vortruba, H. Williams and J. Allison in Birmingham and P. Fourie at SAAO; and our hosts R. Stobie (SAAO); the Carnegie Institution of Washington; the Australia Telescope National Facility (CSIRO); E. J. Rhodes (Mt. Wilson, California); and members (past and present) of the IAC, Tenerife. We would like to thank T. Appourchaux for useful discussions. BiSON is funded by the UK Particle Physics and Astronomy Research Council. WJC was supported by an ESA Internal Fellowship.

REFERENCES

Abrams D., Kumar P., 1996, ApJ, 472, 882
Appourchaux T., Toutain T., Gough D. O., Kosovichev A. G., 1995, in Ulrich R. K., Rhodes E. J., Däppen W, eds, Proceedings of GONG 94, p. 314
Appourchaux T., Chaplin W. J., Elsworth Y., Isaak G. R., McLeod C. P., Miller B. A., New R., 1998a, in Deubner F. -L., ed., Proc. IAU Symp. 185, New Eyes to See Inside the Sun and Stars. Pushing the Limits of Helio- and Asteroseismology with New Observations from Ground and from Space, Kluwer, Dordrecht, p. 45
Appourchaux T. et al., 1998b, in Korzennik S., Wilson A., eds., SOHO6/GONG98 Workshop: Structure and Dynamics of the Interior of the Sun and Sun-like Stars, ESA SP-418. ESA Publications Division, Noordwijk, p. 99
Chaplin W. J., Elsworth Y., Isaak G. R., Lines R., McLeod C. P., Miller B. A., New R., 1997, ApJ, 480, L75
Chaplin W. J., Elsworth Y., Isaak G. R., Lines R., McLeod C. P., Miller B. A., New R., 1998, MNRAS, 300, 1077
Christensen-Dalsgaard J., 1989, MNRAS, 239, 977
Christensen-Dalsgaard J., Proffitt C. R., Thompson M. J., 1993, ApJ, 403, L75
Christensen-Dalsgaard J. et al., 1996, Sci, 272, 1286
Duvall T. L., Jefferies S. M., Harvey J. W., Osaki Y., Pomerantz M. A., 1993, ApJ, 410, 829
Elsworth Y., Howe R., Isaak G. R., McLeod C. P., New R., 1990, Nat, 347, 536
Gabriel M., 1992, A&A, 265, 771
Gabriel M., 1995, A&A, 302, 271
Korzennik S. G., 1998, in Korzennik S., Wilson A., eds, SOHO6/GONG98 Workshop: Structure and dynamics of the Interior of the Sun and Sun-like Stars, ESA SP-418, ESA Publication Division, Noordwijk, p. 933
Kumar P., Basu S., 1999a, ApJ, 519, 389
Kumar P., Basu S., 1999b, ApJ, 519, 396
Nigam R., Kosovichev A. G., 1998, ApJ, 505, L51
Nigam R., Kosovichev A. G., Scherrer P. H., Schou J., 1998, 495, L115
Press W. H., Teukolsky S. A., Vetterling W. T., Flannery B. P., 1992, in Numerical Recipes in Fortran, 2nd edn. Cambridge Univ. Press, Cambridge, p. 407
Rabello-Soares M. C., Appourchaux T., 1999, A&A, 345, 1027
Rast M. P., Bogdan T. J., 1997, ApJ, 496, 527
Rhodes E. J. Jr, Kosovichev A. G., Schou J., Scherrer P. H., Reiter J., 1997, Sol. Phys., 175, 287
Rosenthal C. S., 1998, ApJ, 508, 864
Roxburgh I. W., Vorontsov S. V., 1995, MNRAS, 272, 850
Roxburgh I. W., Vorontsov S. V., 1997, MNRAS, 292, L33
Toutain T., Appourchaux T., 1994, A&A, 289, 649
Toutain T. et al., 1997, Sol. Phys., 175, 311
Toutain T., Appourchaux T., Fröhlich C., Kosovichev A. G., Nigam R., Scherrer P. H., 1998, ApJ, 506, L147
Unno W., Osaki Y., Ando H., Saio H., Shibahashi H., 1989, in Nonradial Oscillations of Stars, 2nd edn. Univ. Tokyo Press, Tokyo, p. 350
Woodard M. F., 1984, PhD thesis, Univ. California, San Diego

This paper has been typeset from a TEX/LATEX file prepared by the author.